Electronic Supplementary Material (ESI) for RSC Advances.

Supporting Information

Construction of Fluorescence Active MOFs with Symmetrical and Conformational Rigid N-2-Aryl-Triazole Ligands

Jingyang Li[a], Ying He[b], Li Wang[a], Guanghua Li[a], Yongcun Zou[a], Yan Yan[a], Dandan Li[a], Xinli Shi[a], Zhiguang Song[*a] and Xiaodong Shi[*b]

a. State key Laboratory of Supramolecular Structure and Materials, College of Chemistry, Jilin University, Changchun, Jilin13002 China; E-mail szg@jlu.edu.cn

b. Department of Chemistry, University of South Florida, 4202 E. Fowler Avenue, Tampa, Florida 33620, United States. E-mail: xmshi@usf.edu

1. General Methods and Materials

All commercial reagents and solvents used during synthesizing ligands and MOFs were directly purchased from Energy Chemical, Bidepharm and Heowns without further purification. Single crystal X-ray diffraction data were obtained from Bruker D8 Venture which was equipped with a MoKα (λ = 0.71073) radiation at 50 kV and 1.2 mA[1]. Powder X-ray diffraction (PXRD) characterizations were processed by Rigaku D/MAX 2550 diffractometer using CuKa radiation at 40 kV and 200 mA. Fourier transform infrared spectroscopy (FT-IR) measurements were carried out by Bruker. Themal gravimetric analyzer (TGA) results were utilized with TA Instrument, TGA Q500 from room temperature to 800 °C. Elemental analysis of carbon, nitrogen and hydrogen (C, H, and N) results were collected from Elementar vario Micro elemental analyzer. Gas adsorption (N_2 and CO_2) were accomplished by ASAP 2020. Fluorescence observations including excitation, emission spectra and quantum yield were completed by Edinburgh Instrument, FLS 920. Nuclear magnetic resonance (NMR) (^{1}H NMR and ^{13}C NMR) spectra were retrieved from a 400 MHz Bruker Avance NEO. At the same time, chemical shifts were analyzed based on internal tetramethylsilane (δ 0.00 ppm) and $CDCl_3$ (δ 7.26 ppm, δ 1.50 ppm) or DMSO (δ 2.50 ppm, δ 3.30 ppm) for ^{1}H data and $CDCl_3$ (δ 77.00 ppm), DMSO (δ 40.00 ppm) for ^{13}C results. HRMS values were summarized by Brucker ESI APCI. Further purification such as column chromatography was performed on 300-400 mesh silica gel.

2. Synthesis of ligands

2.1 General synthetic procedures

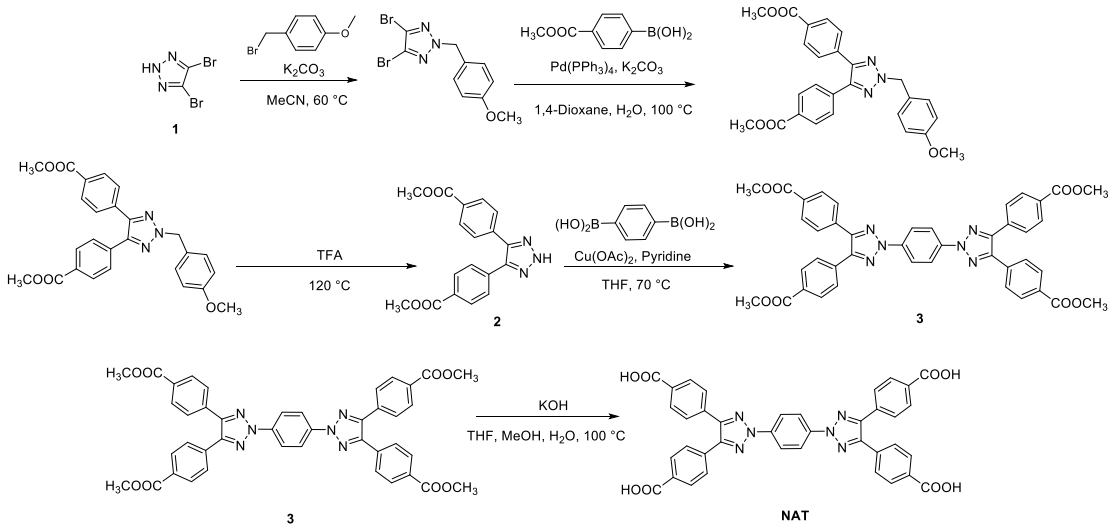

4,5-dibromo-2-(4-methoxybenzyl)-2H-1,2,3-triazole

Mixture of 4,5-dibromo-2H-1,2,3-triazole **1** (5 g, 22 mmol) and K_2CO_3 (12.18 g, 88.16 mmol, 4 equiv.) in MeCN was previously stirred about 30 min before injecting 4-Methoxybenzyl bromide (4.87 mg, 24.22 mmol, 1.1 equiv.) slowly under N_2 at room temperature, and kept stirring at 60 °C for 72 h followed by TLC. After starting molecule converted completely, the reaction mixture was extracted with ethyl acetate and brine for three times. Then, solvent was concentrated under vacuum and product was further purified by silica gel column chromatography (DCM:PE = 1:1) as white solid (yield 98%).

^{1}H NMR (400 MHz, $CDCl_3$) δ 7.31 (d, *J* = 8.7 Hz, 2H), 6.88 (d, *J* = 8.7 Hz, 2H), 5.44 (s, 2H), 3.80 (s, 3H).

^{13}C NMR (101 MHz, $CDCl_3$) δ 159.98, 129.94, 125.91, 124.56, 114.24, 59.77, 55.26.

HRMS (ESI) m/z calcd. for $[C25H35N5O5Si+H]^+$ 345.9112 found 345.3049.

Dimethyl 4,4'-(2-(4-methoxybenzyl)-2H-1,2,3-triazole-4,5-diyl)dibenzoate

4,5-dibromo-2-(4-methoxybenzyl)-2H-1,2,3-triazole (5 g, 14.41 mmol), tetrakis(triphenylphosphine)palladium (0.83 g, 0.72 mmol, 0.05 equiv.), 4-(Methoxycarbonyl)benzeneboronic acid (7.78 g, 43.23 mmol, 3 equiv.) and potassium carbonate (7.97 g, 57.64 mmol, 4 equiv.) were added into a 100 ml Schlenk tube and degassed three times at room temperature. 1,4-dioxane and deionized water (1:1) were eventually poured into tube and increase reaction temperature to 100 °C after repeat degas process. After 12 h, the reaction mixture was extracted with EA and saturated brine and evaporate solvent under vacuum. The mixture was finally purified by silica column chromatography (DCM:EA = 40:1) to obtain white solid product (yield 97%).

^{1}H NMR (400 MHz, $CDCl_3$) δ 8.02 (d, *J* = 8.3 Hz, 1H), 7.60 (d, *J* = 8.4 Hz, 1H), 7.41 (d, *J* = 8.6 Hz, 1H), 6.90 (d, *J* = 8.6 Hz, 1H), 5.59 (s, 1H), 3.92 (s, 2H), 3.79 (s, 1H).

^{13}C NMR (101 MHz, $CDCl_3$) δ 166.61, 159.76, 144.12, 135.20, 129.86, 128.17, 126.87, 114.16, 58.57, 55.23, 52.14.

HRMS (ESI) m/z calcd. for $[C25H35N5O5Si+H]^+$ 458.1638 found 458.1722.

Dimethyl 4,4'-(2H-1,2,3-triazole-4,5-diyl)dibenzoate (2)

Dimethyl 4,4'-(2-(4-methoxybenzyl)-2H-1,2,3-triazole-4,5-diyl)dibenzoate (5 g, 10.93 mmol) was dissolved in concentrated trifluoroacetic acid (20 ml) at 120 °C for 72 h. Saturated sodium bicarbonate was used to wash excessed TFA until pH = 5. Brine and EA were subsequently utilized to extract mixture. The organic phase was concentrated under vacuum and purified through silica column chromatography (DCM:EA = 20:1) as white solid (54% yield).

^{1}H NMR (400 MHz, $CDCl_3$) δ 8.07 (d, *J* = 8.2 Hz, 1H), 7.63 (d, *J* = 8.2 Hz, 1H), 3.94 (s, 3H).

^{13}C NMR (101 MHz, DMSO) δ 166.76, 138.28, 130.11, 128.69, 128.34, 52.76.

HRMS (ESI) m/z calcd. for $[C25H35N5O5Si+H]^+$ 338.1063 found 338.1160.

Tetramethyl 4,4',4'',4'''-(1,4-phenylenebis(2H-1,2,3-triazole-2,4,5-triyl)) tetrabenzoate (3)

2 (1 g, 2.96 mmol), 1,4-phenylenediboronic acid (0.25 g, 1.48 mmol, 0.5 equiv.),

$Cu(OAc)_2$ (0.81 g, 4.45 mmol, 1.5 equiv.) and pyridine (0.47 g, 5.93 mmol, 2 equiv.) were dissolved in anhydrous THF under 1 atm O_2 at 70 °C. After 12 h, the organic solvent was directly purified under vacuum without any extractions and purified by silica column chromatography (DCM:EA = 1:1) as white solid with 50 % yield.
^{1}H NMR (400 MHz, CDCl3) δ 8.34 (s, 4H), 8.10 (d, J = 8.4 Hz, 8H), 7.72 (d, J = 8.4 Hz, 8H), 3.96 (s, 12H).
^{13}C NMR (101 MHz, CDCl3) δ 166.59 (s), 145.80 (s), 134.61 (s), 130.58 (s), 130.04 (s), 128.41 (s), 119.76 (s), 52.30 (s).
HRMS (ESI) m/z calcd. for $[C25H35N5O5Si+H]^+$ 749.2282 found 749.2283.

4,4',4'',4'''-(1,4-phenylenebis(2H-1,2,3-triazole-2,4,5-triyl))tetrabenzoic acid (NAT)
3 (1 g, 1.34 mmol) was obtained from hydrolysis of **2** with potassium hydroxide (0.9 g, 1.6 mmol, 12 equiv.) in THF and MeOH (v/v = 1:1) at 100 °C overnight. The organic phase was washed with DCM and water subsequently. In addition, water phase was acidified with concentrated HCl to pH=1. The white precipitate was then washed again with deionized water and filter under vacuum to collect white solid (yield 90%).
^{1}H NMR (400 MHz, DMSO) δ 13.18 (s, 4H), 8.35 (s, 4H), 8.05 (d, J = 8.3 Hz, 8H), 7.74 (d, J = 8.3 Hz, 8H).
^{13}C NMR (101 MHz, DMSO) δ 167.22 (s), 145.55 (s), 137.91 (s), 133.99 (s), 131.61 (s), 130.10 (s), 128.60 (s), 119.69 (s).
HRMS (ESI) m/z calcd. for $[C25H35N5O5Si+H]^+$ 693.1656 found 693.1708.

3. MOF synthesis and characterizations

3.1 Synthesis of NAT-MOF-Cd

NAT (20 mg, 0.05 mmol) and $Cd(NO_3)_2{\cdot}4H_2O$ (28 mg, 0.094 mmol) were dissolved in DMF (3 ml), EtOH (3 ml), H_2O (3 ml) and HNO_3 (0.6 ml, 2.2 ml HNO_3 in 10 ml DMF) in 10 ml glass vial at 85 °C for three days. There were needle-like transparent crystals at the bottom of vial with 57 % yield. Elemental analysis of C was 51.27 %, H was 4.49 % and N was 11.17 %, respectively. Single crystal data, PXRD and TGA spectra were shown in Table S1 Figure S3(a) and Figure S6(a). FT-IR results between **NAT** and **NAT-MOF-Cd** were also characterized in Figure S5(b).

3.2 Synthesis of NAT-MOF-Cu

The mixture of **NAT** (4,4',4'',4'''-(1,4-phenylenebis(2H-1,2,3-triazole-2,4,5-triyl))tetrabenzoic acid) (20 mg, 0.052 mmol) and $Cu(NO_3)_2{\cdot}3H_2O$ (31 mg, 0.104 mmol) in DMF (3 ml), EtOH (0.6 ml), H_2O (0.6 ml) and 9M Acetic Acid (2.4 ml) were transferred into 10 ml glass vial and kept the reaction at 85 °C for three days. Obviously, blue crystals were obtained with 62 % yield (C: 52.58 % H: 4.41 % N: 12.25 %). Characterizations including single crystal data, PXRD plots, FT-IR and TGA curves spectra were illustrated below,

respectively. (Table S2, Figure S3(b), Figure S5 (b) and Figure S6(b))

3.3 Single Crystal X-Ray Diffraction for NAT-MOFs

The crystallographic data for **NAT-MOF-Cd** and **NAT-MOF-Cu** were collected on a Siemens Smart CCD diffractometer with graphite-monochromated Mo K*α* (λ = 0.71073 Å) radiation at a temperature of 202(2) and 300(2) K respectively. The structure was solved by direct methods with SHELXT [1] and refined by full-matrix least-squares on F^2 using the SHELXTL-2014 [2]. All non-hydrogen atoms were refined with anisotropic displacement parameters. The disordered atoms were refined by ISOR restraint and the Uij values of the displacement parameters for the disordered atoms of coordinated solvent molecules were restrained by SIMU instruction. The hydrogen atoms of the ligands were generated geometrically. All structures were examined using the Addsym subroutine of the PLATON software [2] to assure that no additional symmetry could be applied to the models. The contribution of the electron density associated with disordered solvent molecules was removed by the SQUEEZE routine [3] in PLATON. The final formula was derived from crystallographic data combined with elemental and thermogravimetric analyses data.

References

[1] G.M. Sheldrick, Acta Cryst. (2015). A71, 3–8.
[2] G.M. Sheldrick, Acta Cryst. (2015). C71, 3–8.
[3] A.L. Spek, Acta Cryst. (2015). C71, 9–18.

Table S1 Crystal data and structure refinement for NAT-MOF-Cd.

CCDC number	2024239
Empirical formula	$C_{41}H_{28}CdN_7O_9 \cdot 1.5DMF \cdot 4.5H_2O$
Formula weight	875.10
Temperature/K	202(2)
Crystal system	monoclinic
Space group	I2/c
a/Å	34.010(2)
b/Å	9.0351(5)
c/Å	38.6788(18)
α/°	90
β/°	115.365(4)
γ/°	90
Volume/Å^3	10739.6(11)
Z	8
ρ_{calc}g/cm^3	1.082
μ/mm^{-1}	0.454

F(000)	3544.0
Crystal size/mm^3	0.12 × 0.1 × 0.1
Radiation	MoKα (λ = 0.71073)
2Θ range for data collection/°	4.656 to 50.868
Index ranges	-39 ≤ h ≤ 40, -10 ≤ k ≤ 10, -44 ≤ l ≤ 46
Reflections collected	39663
Independent reflections	9864 [R_{int} = 0.0345, R_{sigma} = 0.0329]
Data/restraints/parameters	9864/20/525
Goodness-of-fit on F^2	1.101
Final R indexes [I>=2σ (I)]	R_1 = 0.0656, wR_2 = 0.1688
Final R indexes [all data]	R_1 = 0.0748, wR_2 = 0.1730
Largest diff. peak/hole / e Å^{-3}	1.05/-1.26

Table S2 Crystal data and structure refinement for NAT-MOF-Cu.

CCDC number	2009548
Empirical formula	$C_{22}H_{16}CuN_4O_5$·DMF·H_2O
Formula weight	479.94
Temperature/K	300(2)
Crystal system	monoclinic
Space group	P2/c
a/Å	12.3238(12)
b/Å	21.6586(19)
c/Å	9.7902(11)
α/°	90
β/°	111.208(3)
γ/°	90
Volume/Å^3	2436.2(4)
Z	4
ρ_{calc}g/cm^3	1.309
F(000)	980.0
Crystal size/mm^3	0.12 × 0.12 × 0.1
Radiation	MoKα (λ = 0.71073)
2Θ range for data collection/°	5.642 to 50.518
Index ranges	-14 ≤ h ≤ 14, -25 ≤ k ≤ 25, -11 ≤ l ≤ 10
Reflections collected	16205
Data/restraints/parameters	4345/320/293
Goodness-of-fit on F^2	1.035
Final R indexes [I>=2σ (I)]	R_1 = 0.0685, wR_2 = 0.2026
Final R indexes [all data]	R_1 = 0.0749, wR_2 = 0.2099

Largest diff. peak/hole / e $Å^{-3}$	1.32/-0.98

Table S3. Hydrogen bonds for NAT-MOF-Cd[A and deg.]

D-H...A	d(D-H)	d(H...A)	d(D...A)	<(DHA)
O8-H8A...O7	0.84	1.85	2.623(10)	152.0
O8-H8A...O7	0.84	1.85	2.623(10)	152.0

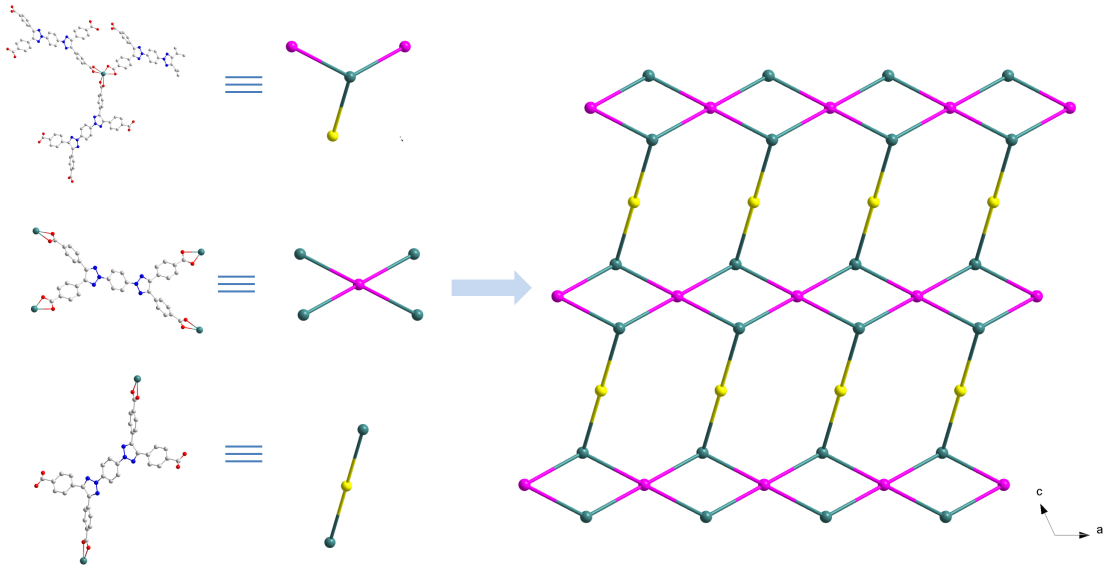

Figure S1. 2,3,4-c topology construction of **NAT-MOF-Cd**.

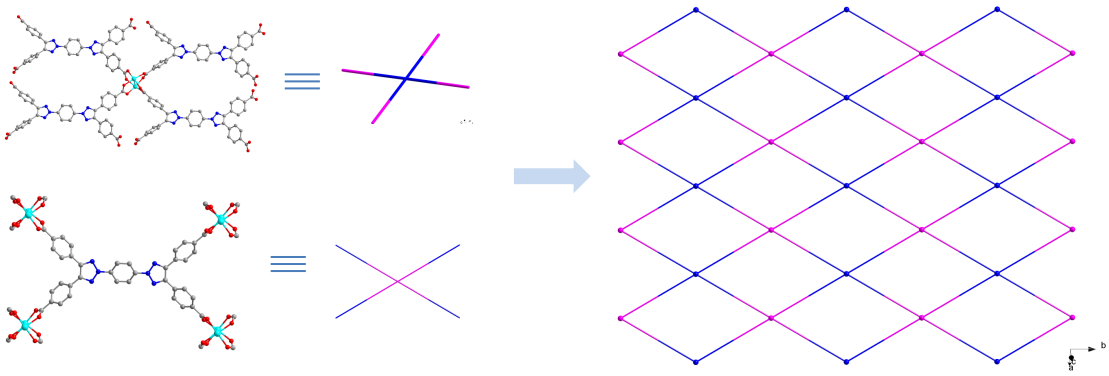

Figure S2. 4-c topology formation of **NAT-MOF-Cu**.

3.4 Powder X-ray diffraction

Powder X-ray diffraction (PXRD) characterizations were processed using CuKa radiation at 40 kV and 200 mA from 4° to 35° at room temperature. Figure S3 demonstrates PXRD curves of NAT-MOFs. Activated **NAT-MOF-Cd** and **NAT-MOF-Cu** are coincident with simulated diagrams and confirms effective synthesis of these two porous

frameworks.

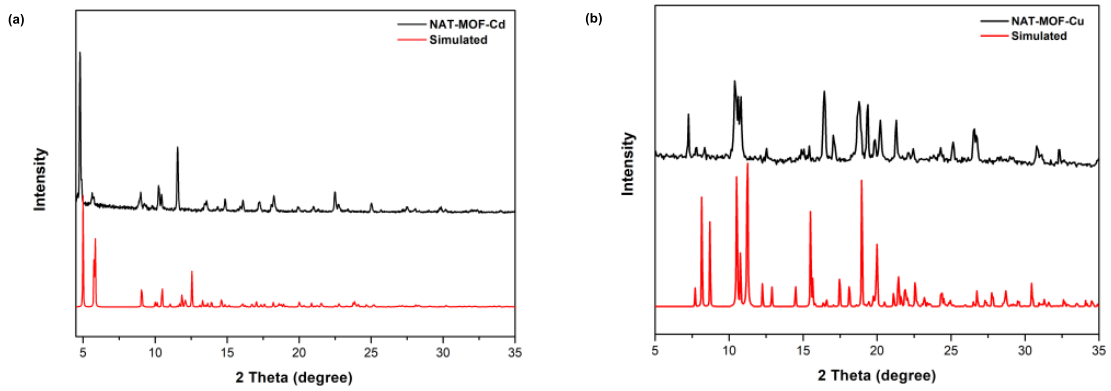

Figure S3. PXRD curves of (a) **NAT-MOF-Cd** and (b) **NAT-MOF-Cu**.

Solvent stability of **NAT-MOF-Cd** was processed by immersing sample into EtOH, MeCN, THF, and DCM at room temperature. New peaks at around 7.5 degree appeared after soaking which indicated the poor stability of **NAT-MOF-Cd** in organic solvent (Figure S4a). As showed by PXRD (Figure S4b), soaking NAT-MOF-Cd in water for only 30 minutes caused total collapse of MOF structures.

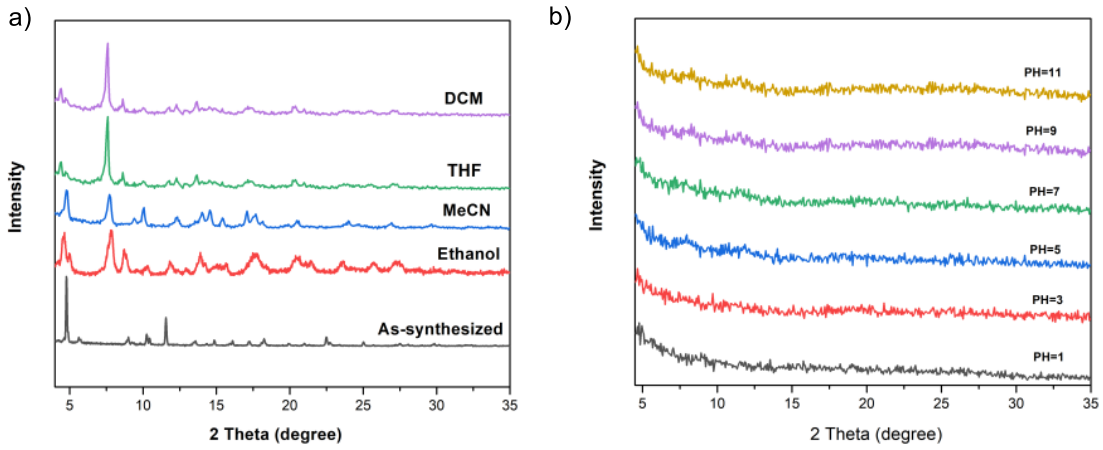

Figure S4. Solvent stability and pH stability of **NAT-MOF-Cd**.

3.5 Fourier transform infrared spectroscopy

Fourier transform infrared spectroscopy (FT-IR) spectra of **NAT**, **NAT-MOF-Cd** and **NAT-MOF-Cu** were analyzed at the same time. For **NAT-MOF-Cd** (Figure S5a), carboxylic acid groups around 2990 cm^{-1} disappeared while the symmetric and asymmetric stretching of carboxylate groups at 1390 cm^{-1} and 1590 cm^{-1} appeared in contrast. For **NAT-MOF-Cu** (Figure S5b), the FT-IR spectra showed the characteristic band of coordinated carboxylate groups at 1394 cm^{-1} and 1581 cm^{-1} and carboxylic acid stretching around 2983 cm^{-1} disappeared consequently.

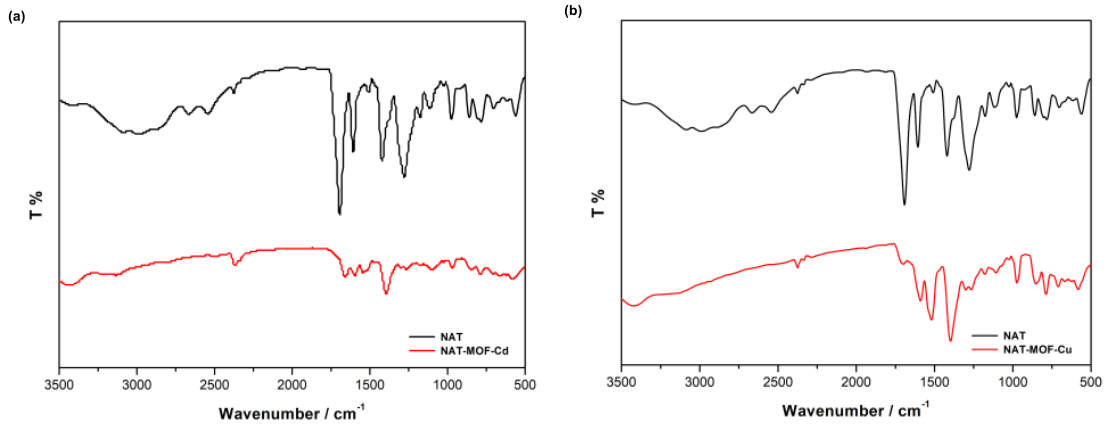

Figure S5. FT-IR spectra of (a) **NAT-MOF-Cd** and (b)**NAT-MOF-Cu**.

3.6 Thermalgravimetric analyses

Thermogravimetric analyses (TGA) were processed from 30 °C to 800 °C. For as-synthesized **NAT-MOF-Cd** (Figure S6a, black curve), the thermal stability was processed in the air and the first weight loss of 7.7 % between 30 °C and 100 °C corresponds to loss of H_2O molecules absorbed on the surface of the scaffold. The successive weight loss of 10.3 % between 100 °C and 356 °C can be concluded to coordinated DMF molecules. Finally, scaffold underwent completely degradation after 356 °C until 592 °C. Meanwhile, thermal stability of **NAT-MOF-Cu** was conducted under N_2 and the first weight loss of 3.2 % happened on **NAT-MOF-Cu** (Figure S6b, red curve) between 30 °C and 100 °C demonstrates loss of H_2O molecules adsorbed on surface of framework. The continuous weight loss of 12.8 % between 100 °C and 363 °C contributes to coordinated DMF molecules. Final weight loss of 58 % between 363 °C and 422 °C refers to collapse of framework. Interestingly, both activated NAT-MOFs show effective guest molecules removal and have similar thermal stability with no decomposition at 354 °C and 351 °C until completely collapse at around 551 °C and 456 °C.

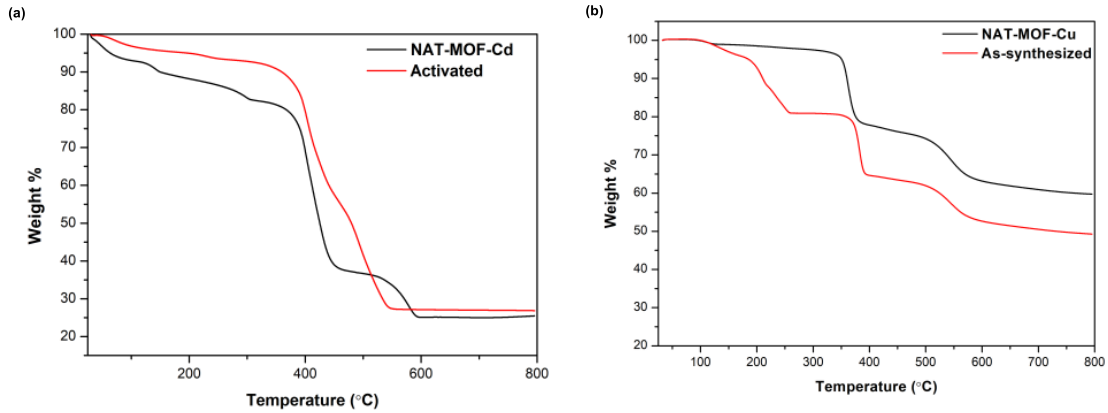

Figure S6. TGA curves of (a) **NAT-MOF-Cd** in the air (b) and **NAT-MOF-Cu** under N_2.

3.7. Gas adsorption experiments

As mentioned before, the N_2 and CO_2 gas adsorption measurements were performed

on a Micromeritics ASAP 2020 (P/P_0 = 0-1.0). **NAT-MOF-Cd** was solvent exchanged with anhydrous EtOH which was changed every one hour for 36 h. **NAT-MOF-Cu** was solvent exchanged with anhydrous MeOH and the same changed the solvent every one hour for 3 days. Then, both **NAT-MOF-Cd** and **NAT-MOF-Cu** were dried under a dynamic vacuum at 85 °C for 24 hours and degas again at 85 °C on the instrument for 12 h before starting the adsorption and desorption tests.

The Brunauer-Emmett-Teller (BET) and Langmuir surface area **of NAT-MOF-Cd** (Figure S8a) was calculated to be 37 $m^2 g^{-1}$ and 55 $m^2 g^{-1}$ for **NAT-MOF-Cd**. Gas adsorption of CO_2 and N_2 for **NAT-MOF-Cd** (Figure S8b) at 273 K were obtained, and CO_2 adsorption was 14 $cm^3 g^{-1}$ for **NAT-MOF-Cd** because of lower pore volumes and unstable framework. Finally, CO_2/N_2 selectivity at 273 K of **NAT-MOF-Cd** was calculated as 8.5.

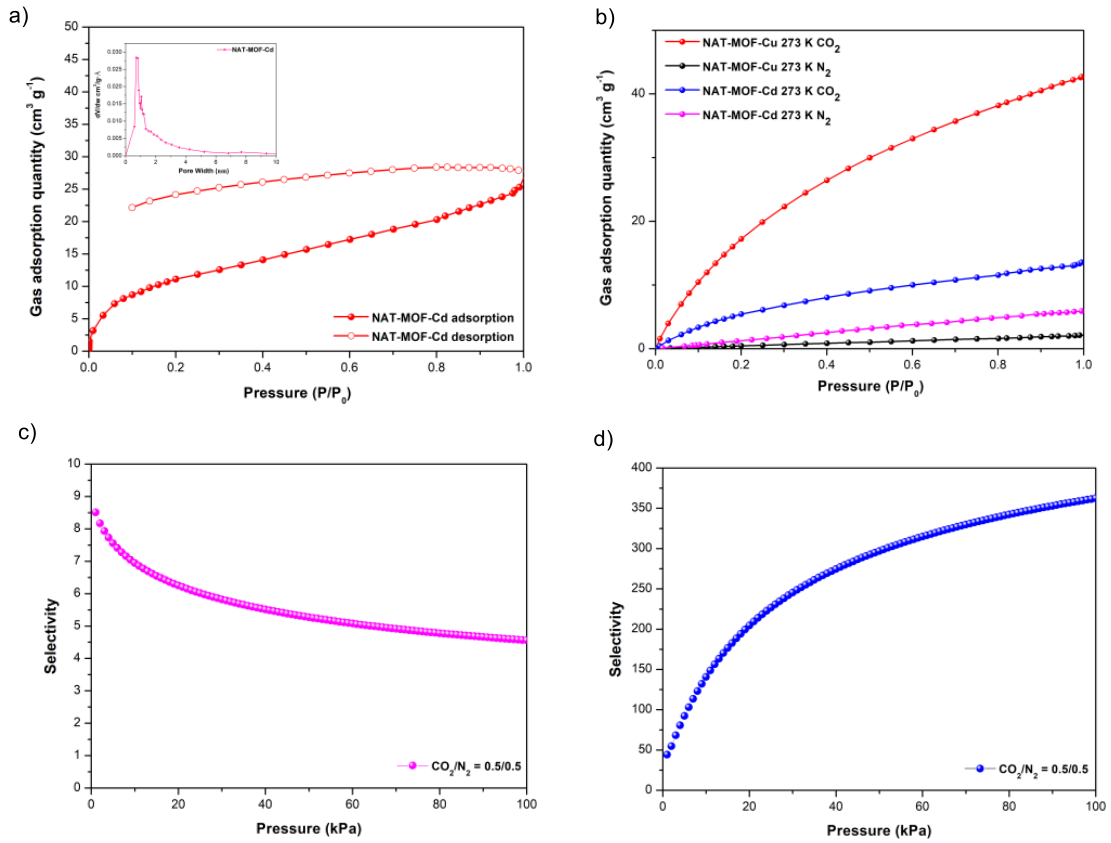

Figure S7. (a) CO_2 sorption of **NAT-MOF-Cd** at 195 K (b) CO_2 and N_2 sorption isotherm of **NAT-MOF-Cu** and **NAT-MOF-Cd** at 273 K; (c) CO_2/N_2 (0.5:0.5) selectivity at 273 K of **NAT-MOF-Cd**; (d) CO_2/N_2 (0.5:0.5) selectivity at 273 K of **NAT-MOF-Cu.**

Table S4. Summary of parameters of the experimentally measured gas adsorption isotherms of **NAT-MOF-Cu.**

T	**273 K CO_2**	**273 K N_2**
R^2	0.99999	0.99961

a1	56.94499	0.23949
a2	1.21089	59.74182
b1	$5.57059E^{-4}$	1.10733
b2	0.02978	0.03462
c1	0.74682	15.84598
c2	1.01583	0.95597

Table S5. Summary of parameters of the experimentally measured gas adsorption isotherms of **NAT-MOF-Cd.**

T	**273 K CO_2**	**273 K N_2**
R^2	0.99979	0.99979
a1	0.69614	0.00186
a2	184.48217	1.17854
b1	0.03107	4247.01494
b2	$6.26942E^{-9}$	0.0017
c1	0.93738	74.2761
c2	2.48124	1.11126

Table S6. Summary of parameters of the experimentally measured Q_{st} of **NAT-MOF-Cu and NAT-MOF-Cd.**

NAT-MOFs	**NAT-MOF-Cu**	**NAT-MOF-Cd**
R^2	0.99994	0.99984
a0	-3471.98699	-3058.6960
a1	42.57068	-8.74038
a2	-288.06405	6.21878
a3	159.46025	-0.32693
a4	-49.02459	0.01164
a5	4.70032	-1.59285E-4
b0	17.38162	13.42301
b1	1.04175	0.00396
b2	0.21062	-0.00746

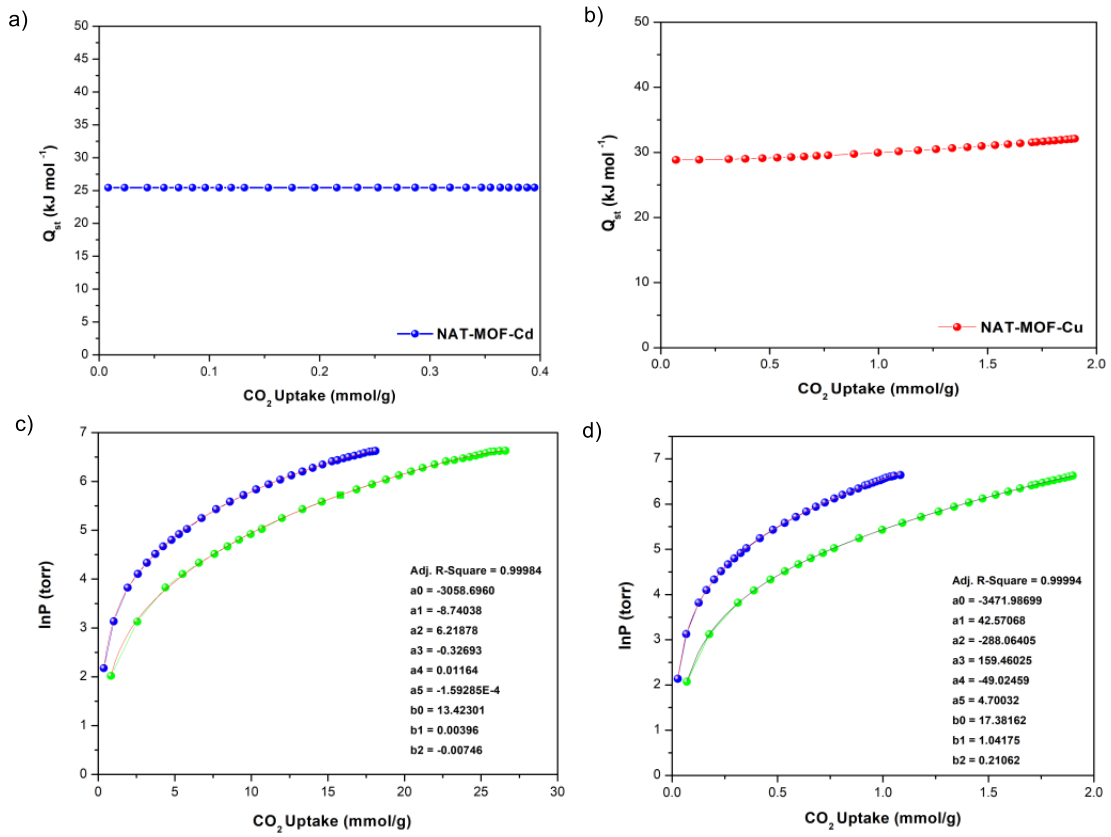

Figure S8. Q_{st} of 273 K CO_2 for **NAT-MOF-Cd** (a,c) and **NAT-MOF-Cu** (b,d).

3.7. Fluorescent properties

Fluorescence detection Procedures: Series fluorescent tests of solid samples of NAT and NAT-MOFs including excitation, emission spectra and quantum yield were completed by Edinburgh Instrument, FLS 920 and were shown in Figure S9. The entrance slit and exit slit were set at 3 nm and 5 nm for the fluorescent determinations with 1 cm cuvette, respectively.

Quantum yield determination: All quantum yields of samples (NAT and NAT-MOFs) were also determined by FLS 920 in the solid state at room temperature under same experimental conditions.

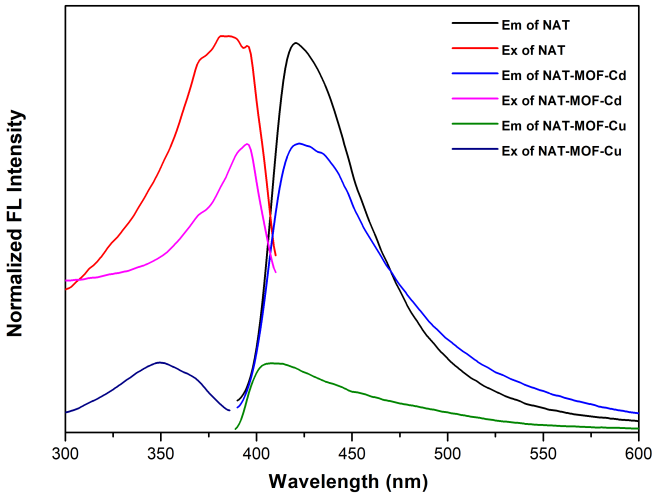

Figure S9. Fluorescence of **NAT,** and NAT-MOFs.

4. NMR Spectra

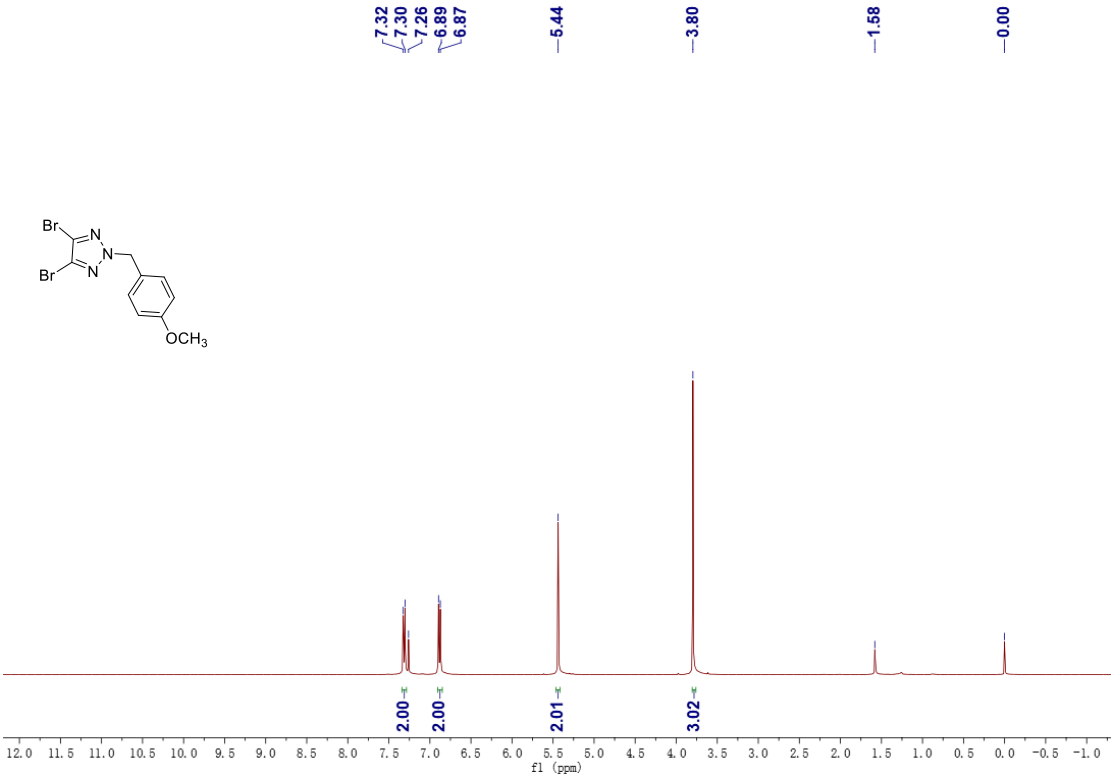

Figure S10. ^{1}**H NMR** spectrum of compound 4,5-dibromo-2-(4-methoxybenzyl)-2H-1, 2,3-triazole.

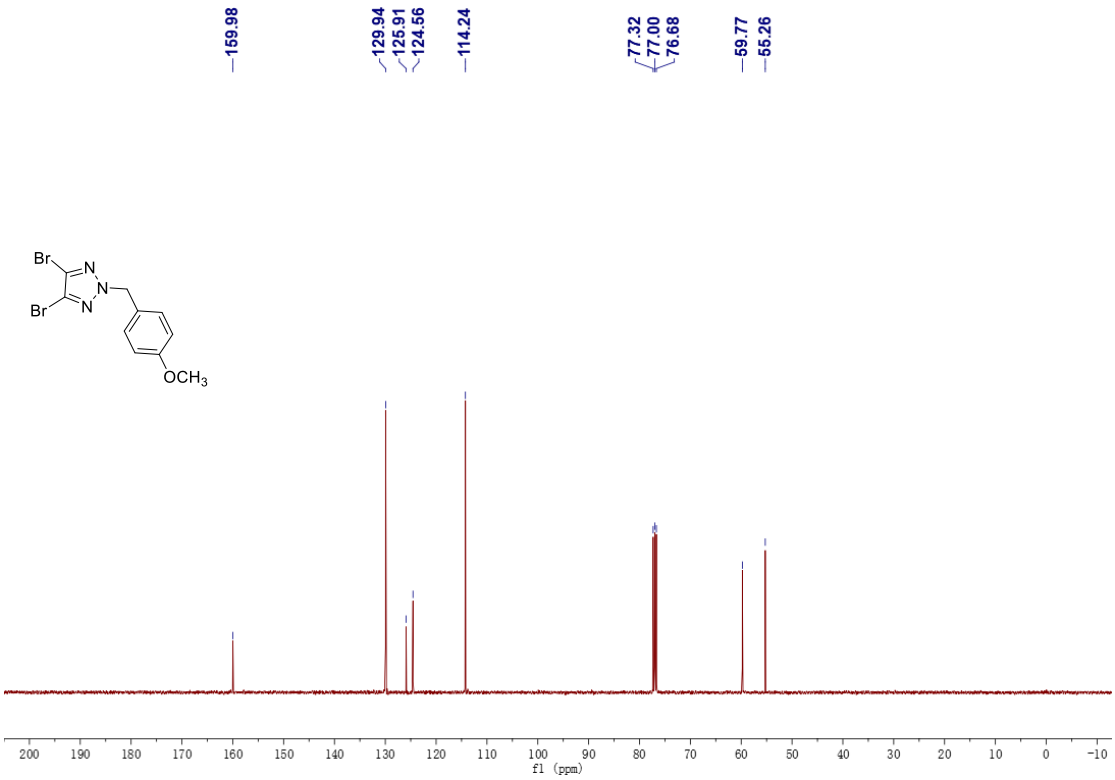

Figure S11. ^{13}C NMR spectrum of compound 4,5-dibromo-2-(4-methoxybenzyl)-2H-1, 2,3-triazole.

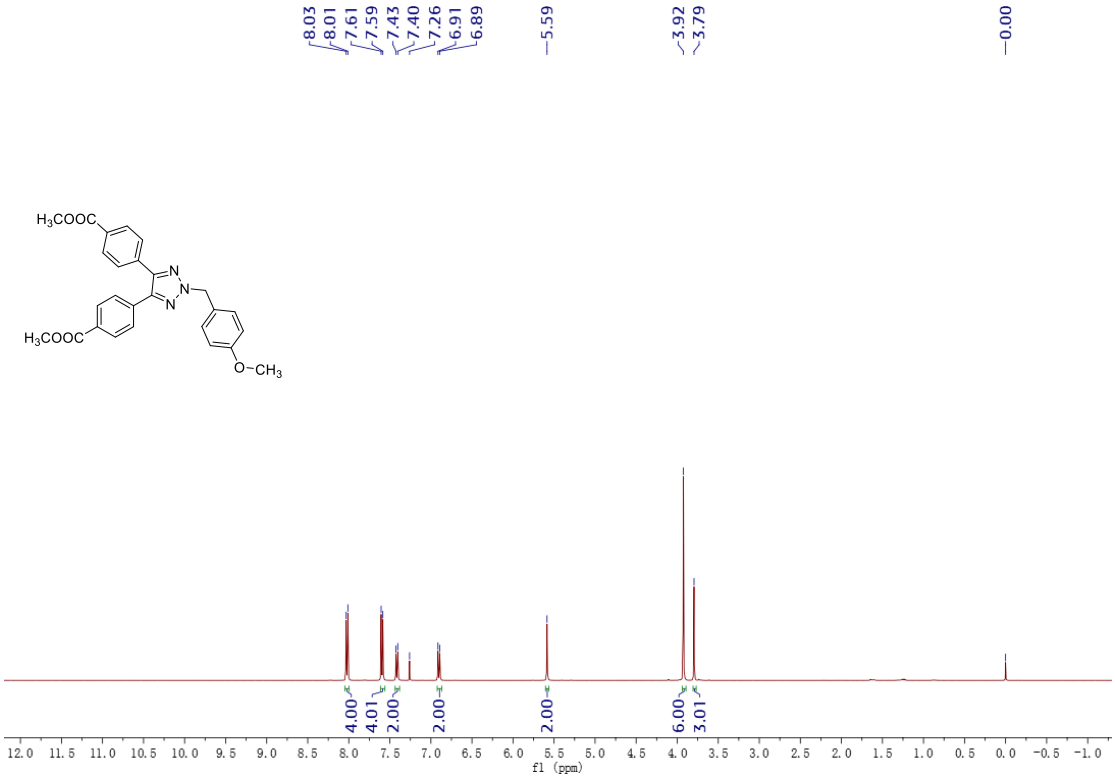

Figure S12. ^{1}H NMR spectrum of compound dimethyl 4,4'-(2-(4-methoxybenzyl)-2H-1,2,3-triazole-4,5-diyl)dibenzoate.

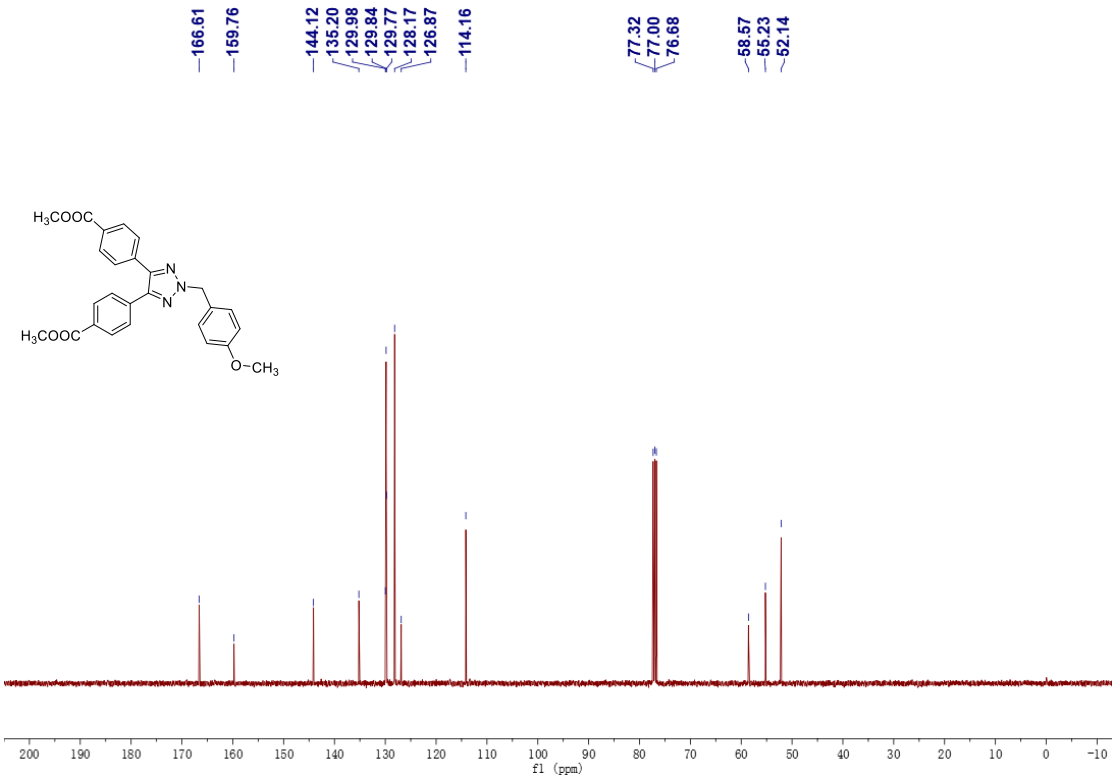

Figure S13. ^{13}C NMR spectrum of compound dimethyl 4,4'-(2-(4-methoxybenzyl)-2H-1,2,3-triazole-4,5-diyl)dibenzoate.

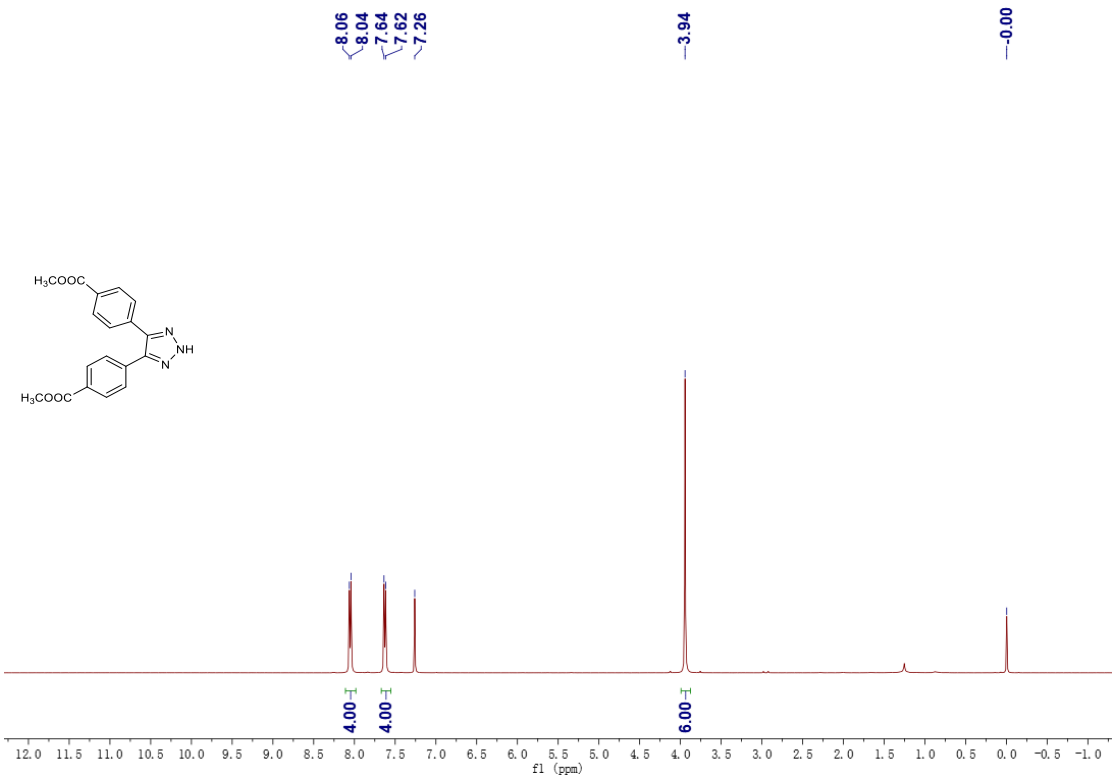

Figure S14. ^{1}H NMR spectrum of compound **2**.

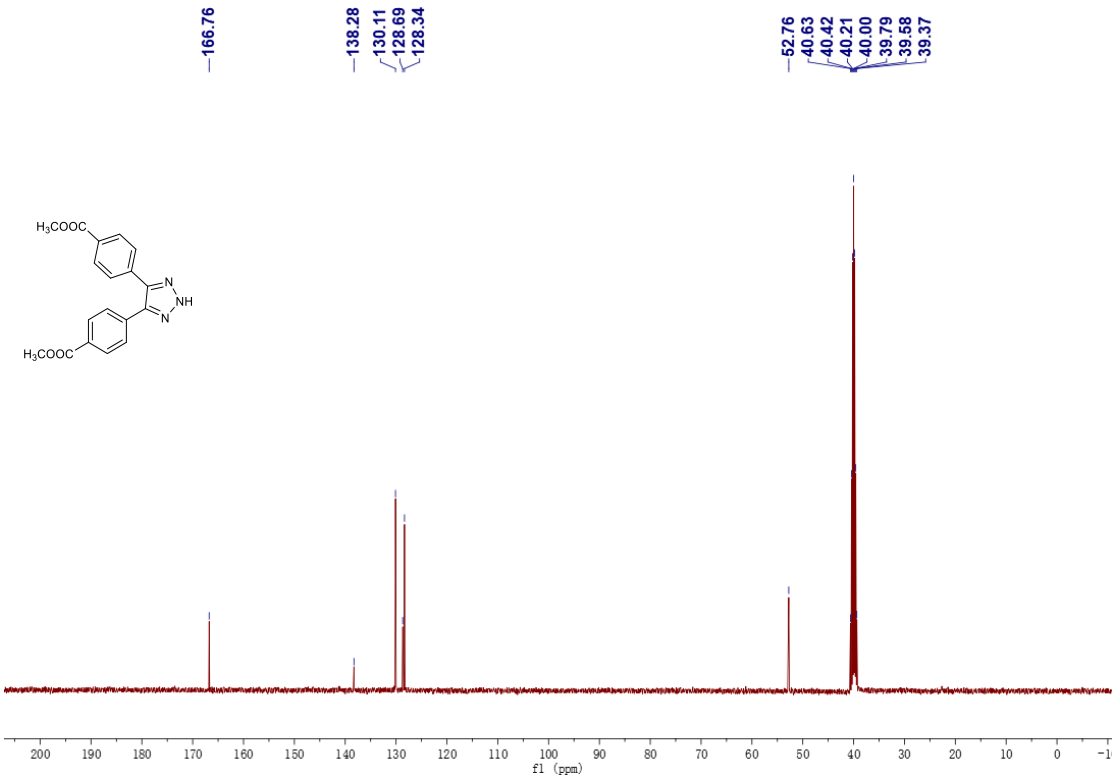

Figure S15. ^{13}C NMR spectrum of compound **2**.

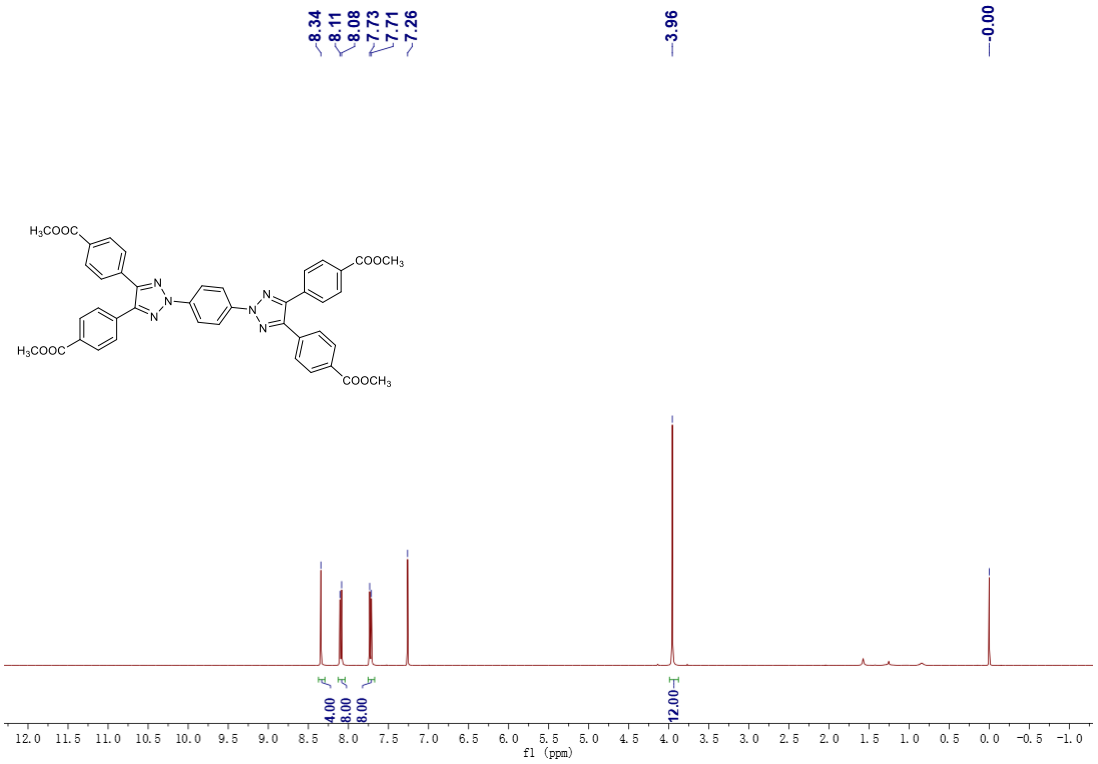

Figure S16. ^{1}H NMR spectrum of compound **3**.

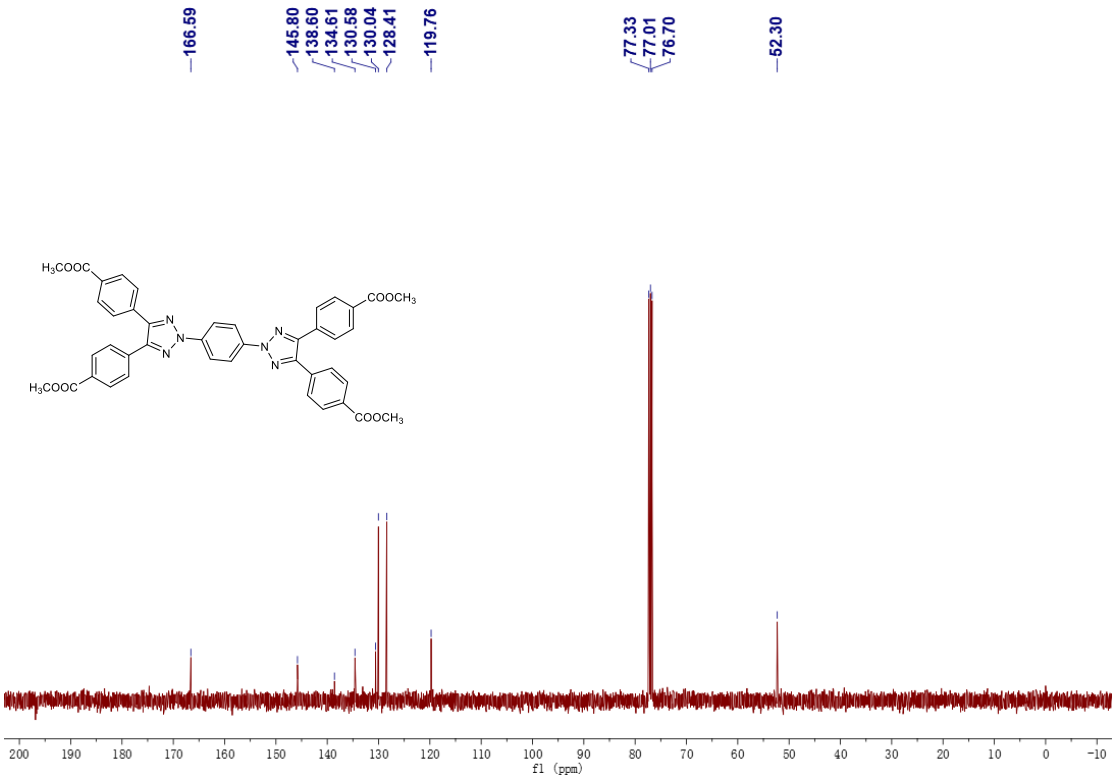

Figure S17. ^{13}C NMR spectrum of compound **3**.

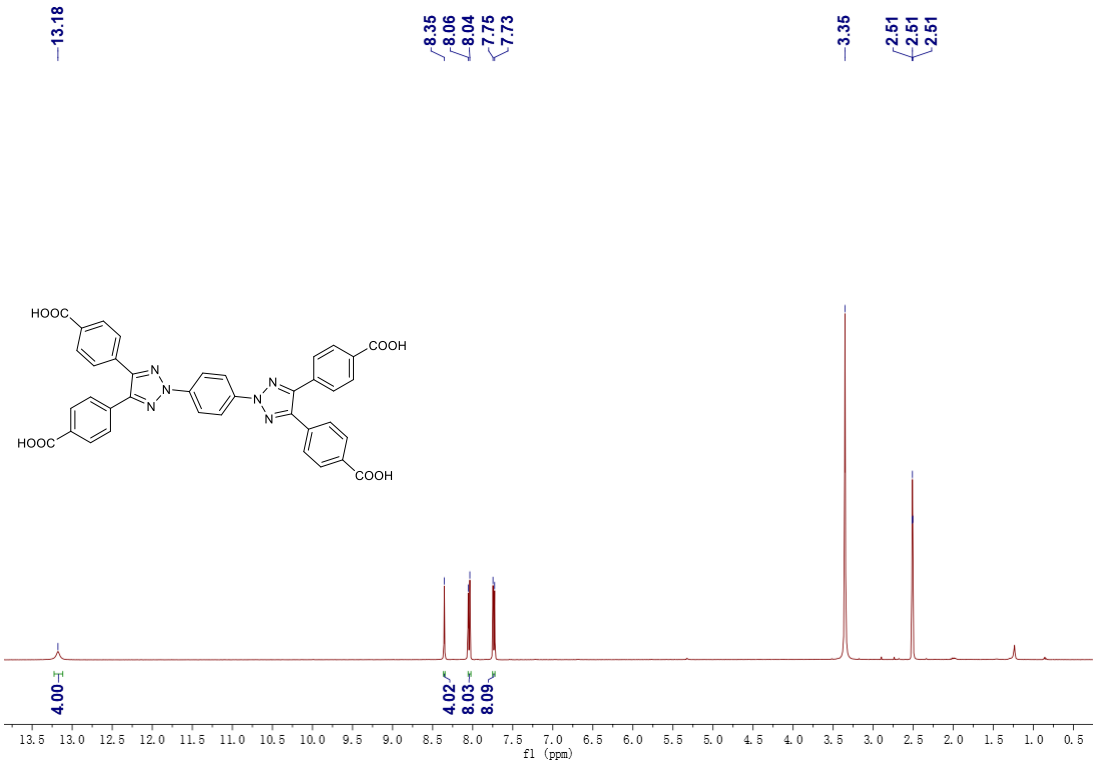

Figure S18. ^{1}H NMR spectrum of compound **NAT**.

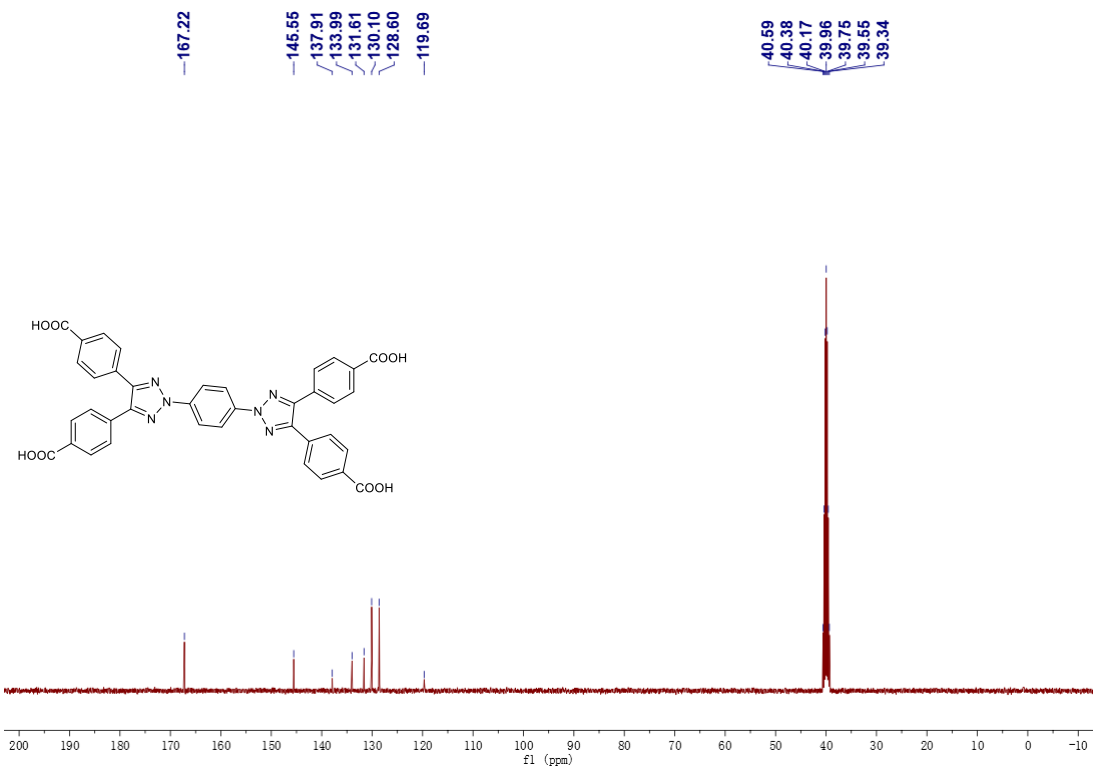

Figure S19. ^{13}**C NMR** spectrum of compound **NAT**.